

Effect of surfactants on single bubble sonoluminescence behavior and bubble surface stabilityThomas Leong,^{1,2} Kyuichi Yasui,³ Kazumi Kato,³ Dalton Harvie,¹ Muthupandian Ashokkumar,^{4,5} and Sandra Kentish^{1,*}¹*Department of Chemical and Biomolecular Engineering, The University of Melbourne, VIC 3010, Australia*²*Faculty of Science, Engineering and Technology, Swinburne University of Technology, Hawthorn, VIC 3122, Australia*³*National Institute of Advanced Industrial Science and Technology (AIST), 2266-98 Anagahora, Shimoshidami, Moriyama-ku, Nagoya 463-8560, Japan*⁴*School of Chemistry, The University of Melbourne, VIC 3010, Australia*⁵*Chemistry Department, King Abdulaziz University, Jeddah, Saudi Arabia*

(Received 30 July 2013; published 8 April 2014)

The effect of surfactants on the radial dynamics of a single sonoluminescing bubble has been investigated. Experimentally, it is observed that an increase in the surfactant concentration leads to a decline in the oscillation amplitude and hence light emission intensity. Numerical simulations support this result, showing that under the driving pressures required to achieve single bubble sonoluminescence (SBSL), the surface properties, namely, the surface elasticity and dilatational viscosity, contribute to the damping of the radial amplitude in the bubble oscillation. In most cases this stabilizes the bubble surface, and contributes to a decreased light intensity. A stronger driving pressure is necessary to achieve equivalent light emission to a surfactant-free bubble. However, as the driving pressure is increased, the surface stability also decreases, making it practically very difficult for a bubble to achieve high SBSL intensities in concentrated surfactant solutions. Although more stable owing to more mild pulsations, the instability mechanism for a surfactant-coated bubble at higher ambient radii is more likely to be of the Rayleigh-Taylor type than that of a clean bubble at the same given acoustic parameters, which can lead to bubble disintegration before correcting mechanisms can bring the bubble back into the stable sonoluminescence regime.

DOI: [10.1103/PhysRevE.89.043007](https://doi.org/10.1103/PhysRevE.89.043007)

PACS number(s): 78.60.Mq, 43.35.Ei, 47.55.dd

I. INTRODUCTION

Sonoluminescence can be produced when a single bubble undergoes extremely nonlinear pulsations within an acoustic field, a phenomenon termed single bubble sonoluminescence (SBSL) [1]. The approach was initially developed by Gaitan [1] whereby a single bubble is levitated in a liquid where an acoustic standing wave exists. A bubble smaller than the resonance size will be drawn towards the pressure antinode due to the *primary Bjerknes* force [2,3] (Fig. 1). Gaitan showed that by partially degassing the liquid and setting the acoustic driving pressure sufficiently high, the bubble can be made to emit sonoluminescence, which can be observed as short pulses of light occurring once every acoustic cycle with “clockwork”-like regularity. The intensity of the emitted light is dependent on various factors that include the amount and type of dissolved gases in the liquid [4], the frequency of the applied ultrasound [5], the applied sound pressure amplitude, hydrostatic pressure, and addition of particular solutes [6–9].

To understand the mechanism of SBSL, many researchers have investigated theoretically the dynamics of single bubbles at conditions where light emission is possible. To account for the highly nonlinear bubble dynamics, terms accounting for thermal and radiation damping need to be included into the Rayleigh-Plesset equation. Researchers have used methods ranging from approximate approaches using adiabatic assumptions [10–12] to in-depth analysis taking into account effects such as thermal conduction [13,14], evaporation and condensation of water vapor into and out of the bubble [15], and chemical reactions of species in solution due to the very

high temperatures expected [16]. Development of these models has enabled researchers to calculate with reasonable accuracy not just the emission of light and temperature [17], but also the formation of sonochemical products [18].

The effects of surfactants, polymers, and alcohols on the radial dynamics and sonoluminescence of a single bubble have been investigated experimentally and numerically. Stottlemeyer and Apfel [19] reported that the surfactant Triton X-100 reduced the maximum size of the single bubble as well as the SL intensity and acoustic emissions. Ashokkumar *et al.* [7] showed that micromolar concentrations of nonvolatile surfactants such as sodium dodecyl sulphate (SDS), dodecyl trimethyl ammonium chloride (DTAC), and dodecyl ammonium propane sulfonate (DAPS) did not significantly affect the dynamics or SL of a single bubble. However, volatile surface active species, such as pentanol, were shown to quench the SL intensity of the bubble by approximately 90% without affecting the bubble dynamics. Numerical simulations performed by Yasui [20] explained that the effect of the surfactant was to inhibit the condensation of water vapor at the bubble wall during bubble collapse. This lowers the achievable temperature inside the bubble due to the presence of more water vapor inside the collapsing bubbles. The high temperature of bubble collapse also raises the possibility that some of the surfactant molecules are dissociated at the bubble wall.

The effect of higher concentrations of surfactant on SBSL, however, has not yet been studied. Higher bulk concentrations of surfactant (below the critical micelle concentration) will result in higher surfactant loadings on the bubble surface [21] and increase the viscoelasticity of the surface [22], which can have a significant effect on the radial dynamics and stability of the bubble. Such effects have been extensively observed in the study of ultrasound contrast agents, where the acoustic

*Corresponding author: sandraek@unimelb.edu.au

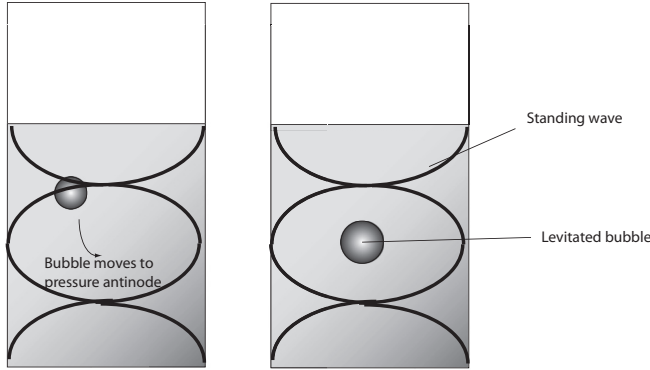


FIG. 1. A standing wave generated inside a cell will cause a bubble below its resonance size to be drawn to the pressure antinode due to the primary Bjerknes force. The bubble located at the antinode will sonoluminesce if driven at a sufficient acoustic pressure and the solution is sufficiently degassed. The light observed is emitted as short pulses once every acoustic cycle.

response or the potential rupture of the surfactant coating is the focus, rather than SBSL [23–34]. Conversely, the current study aims to investigate, experimentally and theoretically, the effect of surfactant upon sonoluminescence.

In these surfactant-rich environments, the shape stability of a bubble is an important concept. Instabilities arise from perturbations of the surface that disrupt the spherical shape of the bubble such that the curvature of the liquid becomes nonuniform and forms a local surface tension pressure associated with each point of the surface [35]. Under stable conditions, these perturbations are dampened and the bubble returns to its equilibrium condition (spherical). However, sometimes, dramatic overshoot and oscillations can occur which can propagate over a large number of cycles, leading to experimentally observed phenomena such as shape mode oscillations [36]. This is referred to as parametric instability [37]. Conversely, Rayleigh-Taylor instability refers to dramatic oscillations that occur at the point of a strong bubble collapse and persist only for a single cycle. Rayleigh-Taylor instabilities are more likely to cause a bubble to move chaotically (dancing motion) and to pinch off daughter bubbles [38] or to disintegrate completely, as the bubble usually does not have enough time to correct the strong perturbation to its surface. For consistent and strong SBSL to occur whereby the bubble is trapped in the pressure antinode, a bubble should oscillate in a stable regime, or in a region of parametric instability.

II. MATERIALS AND METHOD

The surfactants used were of the purest grades available: sodium dodecyl sulphate (SDS) (VWR international, purity > 99%) and dodecyl trimethyl ammonium chloride (DTAC) (TCI Japan, purity > 99%). Sodium chloride (NaCl) was supplied by Merck Germany (purity > 99.5%).

The same apparatus setup as detailed for single bubble rectified diffusion experiments by Leong *et al.* [39] was used with minor adjustments for these experiments (Fig. 2). A vacuum pump was used to partially degas the solution. To avoid excessive foaming that can occur when agitating surfactant

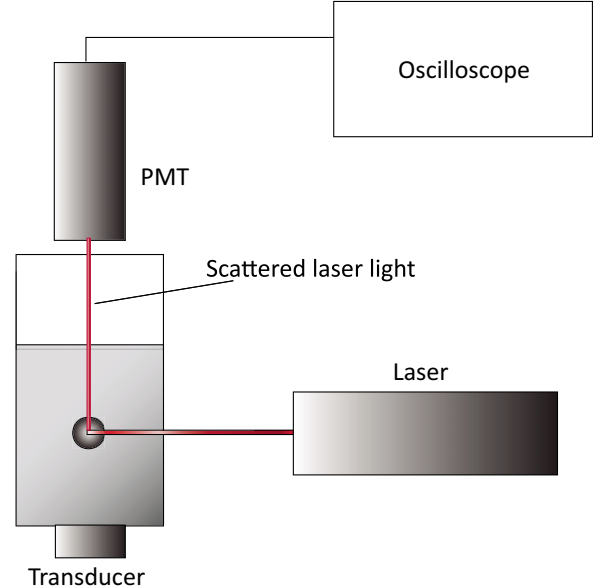


FIG. 2. (Color online) Setup for measuring the SBSL intensity and radial dynamics.

solutions, pure water was initially degassed and then used to make up solutions of the required concentrations by diluting a high concentration (100 mM) stock solution of the required surfactant.

To determine the bubble's radial dynamics, light emitted from a low power laser diode (633 nm) was directed at the bubble and its scattered intensity was measured using a photomultiplier tube (PMT) (Hamamatsu E849-35 amplified by Canberra H. V. Supply Model 3002). The same PMT was also used to measure the sonoluminescence intensity. The PMT signal was relayed to an oscilloscope (LeCroy WaveSurfer 452) and an average over 50 sweeps was taken.

A driving pressure between 1.1 and 1.3 bars and frequency of between 22.23 and 22.31 kHz were used. Slight adjustments in the frequency and/or pressure often had to be made to stabilize the bubble in the system, particularly in surfactant solutions. An oxygen meter (YSI 559) was used to measure gas concentration in the solution.

The maximum bubble radii were determined using images processed in IMAGEJ. The minimum bubble radii could not be determined from the images taken. Instead, an approximate R_{\max}/R_{\min} ratio was determined from the data obtained by the oscilloscope for the reflected laser light, which were plotted in MATLAB for further analysis. The estimated R_{\min} in this case was on the order of 5 μm radius.

III. THEORETICAL BACKGROUND

The dilatational properties of a surfactant layer can be characterized by a surface dilatational modulus [40]:

$$\epsilon = d\sigma/d(\ln A) = \left(\frac{d\sigma}{d \ln \Gamma_{\text{surf}}} \right) \left(\frac{d \ln \Gamma_{\text{surf}}}{d \ln A} \right), \quad (1)$$

which describes the change in the surface tension σ with the fractional change in the area, A , of a given surface element. Here Γ_{surf} is the surface excess concentration of surfactant and

σ is the surface tension. The modulus reflects the ability of the surface to retain an excess or deficit of surfactant molecules at the surface such that it is at a nonequilibrium state. A value of zero for this modulus means that the surface is nonelastic and surface tension is constant throughout the perturbation process. In other words, there is no resistance to compression or expansion and equilibrium is reached instantaneously.

The surface elasticity and viscosity can be estimated using a model developed by Lucassen and Van Den Tempel [41] (LT model) which assumes that the surfactant relaxation processes at the bubble interface are governed by Fickian diffusion.

In this case, the surface dilatational modulus can be further broken down into a real and imaginary component corresponding to the surface elastic and viscous responses, respectively:

$$\epsilon = \chi + i\kappa_s\omega, \quad (2)$$

where ω is the angular frequency of oscillation, χ is referred to as the surface elasticity, and κ_s the surface dilatational viscosity. In turn,

$$\chi = \epsilon_0 \frac{1 + \Omega}{1 + 2\Omega + 2\Omega^2}, \quad (3)$$

and

$$\kappa_s\omega = \epsilon_0 \frac{\Omega}{1 + 2\Omega + 2\Omega^2}, \quad (4)$$

where

$$\epsilon_0 = -d\sigma/d(\ln\Gamma_{\text{surf}}), \quad (5)$$

and

$$\Omega = \left(\frac{D}{2\omega}\right)^{1/2} \left(\frac{dc}{d\Gamma_{\text{surf}}}\right). \quad (6)$$

In this final equation, D is the diffusion coefficient for the surfactant in solution and c is the bulk surfactant concentration.

The LT model [40,41] was specifically developed to predict the surface rheological properties of nonionic surfactant solutions or solutions of ionic surfactants with charge suppressed via the addition of salt. Bonfillon and Langevin show that this model may be less accurate for electrolytes in the absence of salt. Furthermore, this model was shown to be valid only for low frequency perturbations (2 Hz). Wantke *et al.* [42] attempted to validate the model in the medium frequency range (on the order of 3–500 Hz). They noted that differences between the experimental results and the model could be attributed to the model only accounting for the surface tension from a monolayer of surfactant molecules. Under dynamic conditions, this criterion may not be fulfilled and the thickness of the surfactant layer should be accounted for, possibly by implementing a volume model with a fixed thickness of the surface phase.

For bubbles subject to ultrasound, the rate of perturbations is on the order of 20 kHz and above. The limiting behavior for a fast oscillating surface would be that the “phase difference” observed between the surface tension variation and the change in area during oscillation [43] approaches zero. At such frequencies, a measurement technique based on the “maximum bubble pressure method” has been used to determine the surface dilatational viscosity of SDS surfactant, valid for

frequencies up to 80 kHz [44]. The dilatational viscosity for SDS surfactant at a bulk concentration of 1 mM was determined to be on the order of 1×10^{-8} N/m s.

In the present study, we use the LT model only to estimate the values of the surface elasticity and viscosity. The estimated values are of the same order of magnitude as those reported by Bonfillon and Langevin [40], Wantke *et al.* [42], and Kao *et al.* [44].

IV. EQUATION OF MOTION

The equation of motion for the radius of a bubble in an acoustic field is a modified Keller equation adapted from Yasui [45]:

$$\begin{aligned} & \left(1 - \frac{\dot{R}}{c_\infty} + \frac{\dot{m}}{c_\infty\rho_L}\right) R\ddot{R} + \frac{3}{2}\dot{R}^2\left(1 - \frac{\dot{R}}{3c_\infty} + \frac{2\dot{m}}{3c_\infty\rho_L}\right) \\ &= \frac{1}{\rho_L}\left(1 + \frac{\dot{R}}{c_\infty}\right)\left[p_B - p_s\left(t + \frac{R}{c_\infty}\right) - p_\infty\right] \\ &+ \frac{\ddot{m}R}{\rho_L}\left(1 - \frac{\dot{R}}{c_\infty} + \frac{\dot{m}}{c_\infty\rho_L}\right) + \frac{\dot{m}}{\rho_L}\left(\dot{R} + \frac{\dot{m}}{2\rho_L} + \frac{\dot{m}\dot{R}}{2c_\infty\rho_L}\right) \\ &+ \frac{R}{\rho_L} \frac{dp_B}{dt}. \end{aligned} \quad (7)$$

Here time derivatives are denoted by a dot with R the radius, \dot{m} the net rate of evaporation (or condensation) of water vapor in the bubble, c_∞ the speed of sound in the bulk (1483 m/s), ρ_L the bulk liquid density (1000 kg/m³), p_s the acoustic field defined as $P_a \cos(\omega t)$ where P_a is the acoustic driving pressure and ω is the angular frequency, and p_∞ the static pressure.

The liquid pressure on the external surface of the bubble is $p_B(t)$ and is related to $p(t)$ by [30]

$$\begin{aligned} p_B(t) = p(t) &- \frac{2\sigma(R_o)}{R} - \frac{4\mu}{R}\left(\dot{R} - \frac{\dot{m}}{\rho_L}\right) - \dot{m}^2\left(\frac{1}{\rho_L} - \frac{1}{\rho_G}\right) \\ &- 4\chi\left(\frac{1}{R_0} - \frac{1}{R}\right) - \frac{4\kappa_s}{R^2}\left(\dot{R} - \frac{\dot{m}}{\rho_L}\right), \end{aligned} \quad (8)$$

where χ is again the surface elasticity, κ_s is the surface dilatational viscosity, and μ is the bulk liquid viscosity.

Marmottant *et al.* [30] argue that Eq. (8) is only valid within a limited range. That is, as the bubble radius reduces, high loadings of surfactant at the interface can lead to an unstable situation where the monolayer buckles out of plane and the surface tension reduces to zero. However, buckling has only ever been observed with insoluble surfactants and is unlikely to occur with soluble surfactants. Rather, for soluble surfactants, compression of the bubble beyond the maximum that can be packed into the interface is likely to expel some molecules into the bulk solution. Hence, in the present analysis, we do not account for bubble buckling.

Similarly, Marmottant *et al.* [30] argue that as the bubble radius increases, the surfactant layer can break up into regions of bare gas interface and regions of surfactant rafts. Once this occurs, the surface tension relaxes to that of water (~ 73 mN/m). However, Marmottant *et al.* [30] argue that the surface tension at which this occurs can be higher than that of water, and indeed can be in excess of 1000 mN/m. In the

present case, the surface tension, calculated by

$$\sigma(R) = \sigma(R_0) + 2\chi \left(\frac{R}{R_0} - 1 \right), \quad (9)$$

never exceeds 350 mN/m for the conditions studied here. Hence shell rupture is ignored.

The gas pressure is obtained from a form of the van der Waals equation of state modified to take into account the inertial effects of the gas [46]:

$$p(t) = \frac{N_{\text{tot}} k_B \langle T \rangle}{V - N_{\text{tot}} B} - \frac{1}{2} \langle \rho_G \rangle R \ddot{R}, \quad (10)$$

where $\langle \rho_G \rangle$ is the volume-averaged gas density, N_{tot} is the total number of gas molecules, k_B the Boltzmann constant ($1.3807 \times 10^{-23} \text{ m}^2/\text{s}^2 \text{ K}$), and B the molecular covolume ($5.1 \times 10^{-29} \text{ m}^3$).

The net rate of evaporation of water vapor \dot{m} is calculated by the following equations [45]:

$$\dot{m} = \dot{m}_{\text{eva}} - \dot{m}_{\text{con}}, \quad (11)$$

$$\dot{m}_{\text{eva}} = \frac{10^3 N_A}{M_{\text{H}_2\text{O}}} \frac{\alpha_M}{(2\pi R_v)^{1/2}} \frac{p_v^*}{T_0^{1/2}}, \quad (12)$$

$$\dot{m}_{\text{con}} = \frac{10^3 N_A}{M_{\text{H}_2\text{O}}} \frac{\alpha_M}{(2\pi R_v)^{1/2}} \frac{\Gamma p_v}{T^{1/2}}, \quad (13)$$

where \dot{m}_{eva} (or \dot{m}_{con}) is the molecular rate of evaporation (or condensation) per unit area and unit time. This means that the net rate of evaporation is the difference between the actual rate of evaporation and that of condensation. The accommodation coefficient for evaporation or condensation, α_M , is calculated by interpolating the results of molecular dynamics simulation by Matsumoto (private communication reported in the work by Yasui [45]) by the Gregory-Newton formula of interpolation [47]:

$$\alpha_m = 0.35 - 0.05k^{(1)} - 0.05k^{(2)} + 0.025k^{(3)}, \quad (14)$$

where

$$k = [T_{L,i}(K)/50] - 7, k^{(m)} = k(k-1) \cdots [k - (m-1)].$$

The equation is valid when $350 \text{ K} \leq T_{L,i} \leq 500 \text{ K}$. The values above 500 K are assumed to be those determined at 500 K. The values below 350 K are assumed to be those determined at 350 K in the present calculations.

$M_{\text{H}_2\text{O}}$ is the molecular weight of water, R_v is the gas constant of water vapor (461.5 J/kg K), p_v^* is the saturated vapor pressure at temperature T_0 , and p_v is the partial pressure of water such that

$$p_v = \frac{n_{\text{H}_2\text{O}}}{n_i} p. \quad (15)$$

Γ is a correction factor taken from Yasui [45] and is expressed as

$$\Gamma = \exp(-\Omega^2) - \Omega \sqrt{\pi} \left[1 - \frac{2}{\sqrt{\pi}} \int_0^\Omega \exp(-x^2) dx \right], \quad (16)$$

in which

$$\Omega = \frac{\dot{m}}{p_v} \left(\frac{R_v T}{2} \right)^{1/2}. \quad (17)$$

To determine the interfacial gas bubble temperature, T , in this model, we follow a similar approach as used by Stricker *et al.* [46] and make no attempt to describe the spatial distribution of the temperature inside the bubble. Instead this is formulated in terms of a volume-averaged value $\langle T \rangle$, determined by a global balance over the bubble volume based on the first principle of thermodynamics,

$$c_v m_g \langle \dot{T} \rangle = Q - p \dot{V}. \quad (18)$$

Here m_g is the mass of gas inside the bubble, c_v is the constant volume specific heat of the gas, and V is the bubble volume. The net heat absorbed by the bubble per unit time is modeled as

$$Q = 4\pi R^2 \lambda_{\text{air}} \frac{T_\infty - \langle T \rangle}{l_{\text{th}}}, \quad (19)$$

where λ_{air} is the approximate thermal conductivity of air determined from [48]

$$\lambda_{\text{air}} = 0.01165 + 5.528 \times 10^{-5} T, \quad (20)$$

valid in the temperature range $200 \text{ K} \leq T \leq 3000 \text{ K}$.

The variable l_{th} here is an estimate of the thickness of the thermal boundary layer in the liquid. This length is estimated to be [45]

$$l_{\text{th}} = n_i \lambda, \quad (21)$$

where $n_i = 7$ and λ is the mean free path of a gas vapor molecule such that

$$\lambda = \frac{V}{\sqrt{2.0} \sigma' N_{\text{tot}}}. \quad (22)$$

In Eq. (22), σ' is the cross sectional area of a molecule in the bubble (in this calculation $\sigma' = 0.4 \times 10^{-18} \text{ (m}^2\text{)}$) is used [49]).

The effects of evaporation, condensation, and thermal conduction can become important for strongly nonlinear collapses when a bubble is subject to a high driving pressure, as occurs under SBSL conditions. As has been shown by Yasui [49], these effects can have an important influence on the bubble dynamics under such conditions. In this analysis, we assume that no chemical reactions take place in the bubble and that the number of molecules of air inside the bubble remains constant during bubble oscillation.

V. STABILITY EQUATION

The instabilities caused by small distortions of the spherical interface can be modeled by Eq. (23) [50]:

$$R_D = R(t) + a_n(t) Y_n(\theta, \phi), \quad (23)$$

where R_D is the bubble radius distorted by bubble oscillations, $R(t)$ is the instantaneous bubble radius governed by the radial time behavior of the oscillating bubble [i.e., the solution to Eq. (7)], Y_n is a spherical harmonic of degree n with $n \geq 0$, and a_n is the radial distortion amplitude for mode n . The aim here is to determine $a_n(t)$, the radial distortion amplitude, which can be used to determine the stability of a bubble. In response to an initial radial perturbation, a stable bubble will have $a_n(t)$ always smaller than $R(t)$ and converging to a finite value, whereas an unstable bubble will have $a_n(t)$ diverge to a value larger than $R(t)$.

The value of $a_n(t)$ is determined by solving the second order ordinary differential equation (24) for $n \geq 0$:

$$\ddot{a}_n + B_n(t)\dot{a}_n - A_n(t)a_n = 0. \quad (24)$$

Loughran *et al.* [51] present equations for $A_n(t)$ and $B_n(t)$ as follows:

$$\begin{aligned} A_n = (n-1) \frac{\ddot{R}}{R} - \frac{(n-1)(n+1)(n+2)\sigma(R_o)}{\rho_L R^3} \\ - \left[\frac{2\mu\dot{R}}{\rho_L R^3} \right] \left[(n-1)(n+2) + 2n(n+2)(n-1) \frac{\delta}{R} \right] \\ - \frac{2n(n+2)\dot{R}\mu_s}{(n+1)R^4\rho_L} [n(n+1) + (n-1)] \\ - \frac{2\kappa_s\dot{R}}{(n+1)\rho_L R^4} [n^2(n+2)(n+1) + 7n^3 + 9n^2 - n - 4] \\ - \chi \left\{ \frac{1}{R^3\rho} (n+2)(n^2 + 4n + 2) \right. \\ \left. + \frac{2(R-R_o)}{(n+1)\rho_L R^4} [n^2(n+2)(n+1) + 7n^3 + 9n^2 - n - 4] \right\} \\ - G_s \left\{ \frac{n(n+2)}{(n+1)R^3\rho_L} [n(n+1) - 2] \right. \\ \left. + \frac{2n(n+2)(R-R_o)}{(n+1)R^4\rho_L} [n(n+1) + (n-1)] \right\}, \quad (25) \\ B_n = \frac{3\dot{R}}{R} + \frac{2\mu}{\rho_L R^2} \left[(n+2)(2n+1) - 2n(n+2)^2 \frac{\delta}{R} \right] \\ + \frac{n(n+2)\mu_s}{(n+1)R^3\rho_L} [n(n+1) - 2] \\ + \frac{\kappa_s}{(n+1)R^3\rho_L} (n+2)(n+1)(n^2 + 4n + 2). \quad (26) \end{aligned}$$

Here ρ_L is the density of the liquid and δ is the diffusive boundary layer thickness around the bubble approximated by

$$\delta = \min\left(\sqrt{\frac{\eta}{\rho_L \omega}}, \frac{R}{2n}\right). \quad (27)$$

These expressions include the effect upon the bubble stability of the surface elasticity (χ) and the surface dilatational viscosity (κ_s), as well as the equilibrium surface tension (R_o) and the bulk liquid viscosity (μ). Loughran *et al.* [51] indicate that these terms are appropriate for describing simple outward expansion of the shell but do not describe the shell bending and flexing. They include the surface shear viscosity (μ_s) and the surface shear modulus (G_s) to account for this bending and flexing. As we cannot estimate these parameters in the present case, we consider two cases:

- (i) G_s and μ_s are zero;
- (ii) G_s and μ_s are 25% of the value of χ and κ_s , respectively.

This is consistent with the values provided by Loughran *et al.* [51].

As the mode $n = 2$ is the least stable of the shape oscillation modes, our stability analysis will focus on this mode. The solution to the radial dynamics is obtained numerically using Euler's method. The behavior is analyzed by the response of the bubble to an initial radial perturbation of 1×10^{-9} m.

The point of instability is determined by adjusting the ambient radius (R_o) for a given acoustic driving pressure until the value of a_2/R first diverges to a value larger than 1. Sample plots

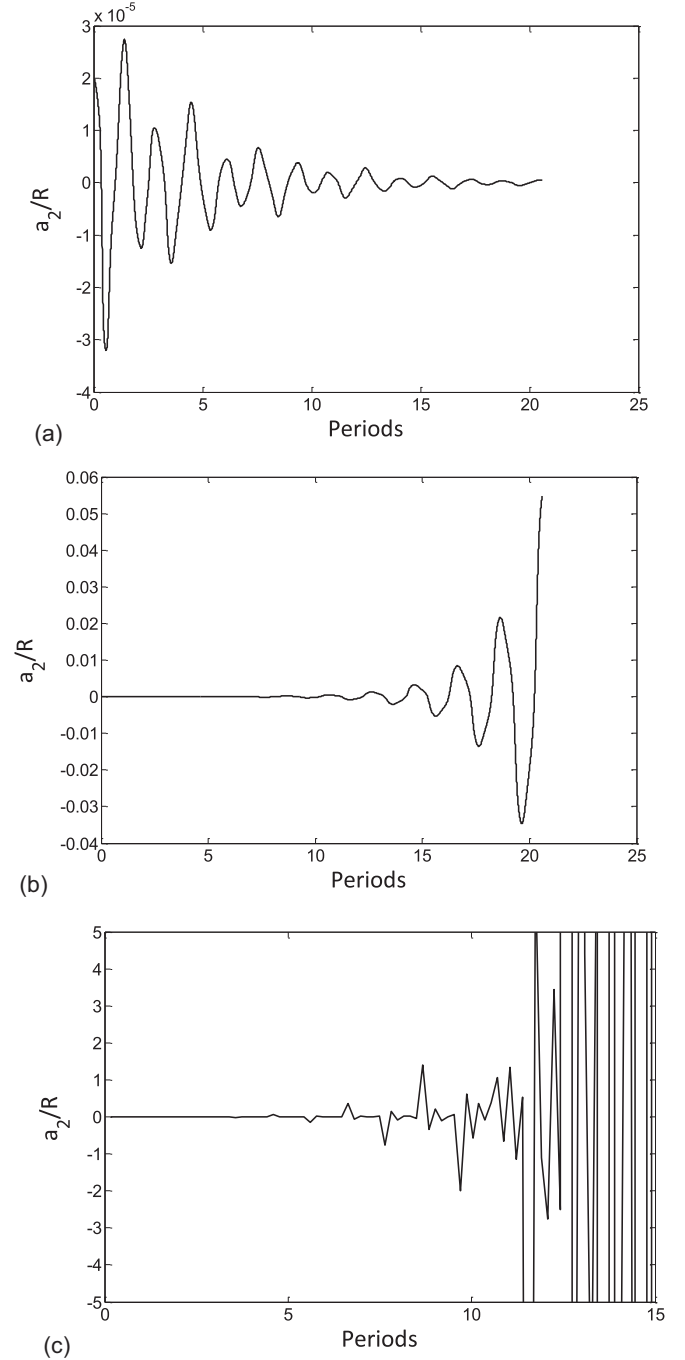


FIG. 3. (a) Plot of a calculated stable bubble surface where the perturbation converges to zero. The bubble has an initial radius of $50 \mu\text{m}$ and a driving pressure of 0.27 bar. (b) Plot of a calculated unstable bubble surface where the perturbation diverges over time. The bubble has an initial radius of $60 \mu\text{m}$ and a driving pressure of 0.27 bar. (c) Plot of the radial distortion amplitude of the $n = 2$ mode for a $2.9 \mu\text{m}$ bubble insonated at 1.7 MHz driven at 400 kPa with shell coating parameters similar in magnitude to those reported by Loughran *et al.* [51] with shell viscosities (κ_s and μ_s) chosen to be 3×10^{-9} and 0.75 N/m s and elasticities (χ and G_s) 500 and 100 mN/m , respectively.

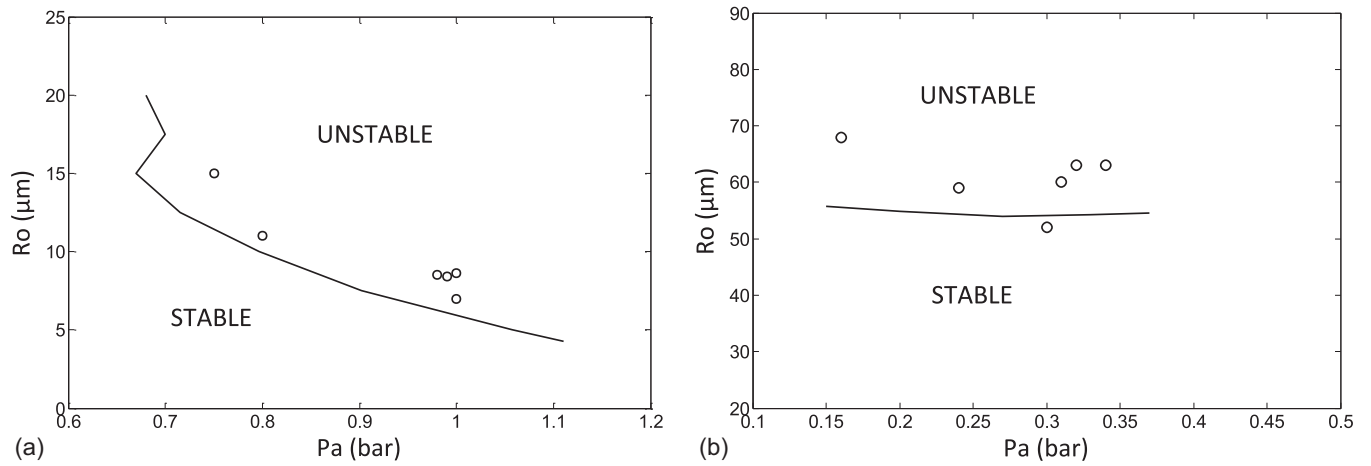


FIG. 4. Plot of the calculated stability boundary for $n = 2$ mode in water at 20.6 kHz. The open marker points are the corresponding experimental data of Holt and Gaitan [10] for (a) higher driving pressures, (b) at lower driving pressures at which a bubble is observed to first become unstable (i.e., stability boundary).

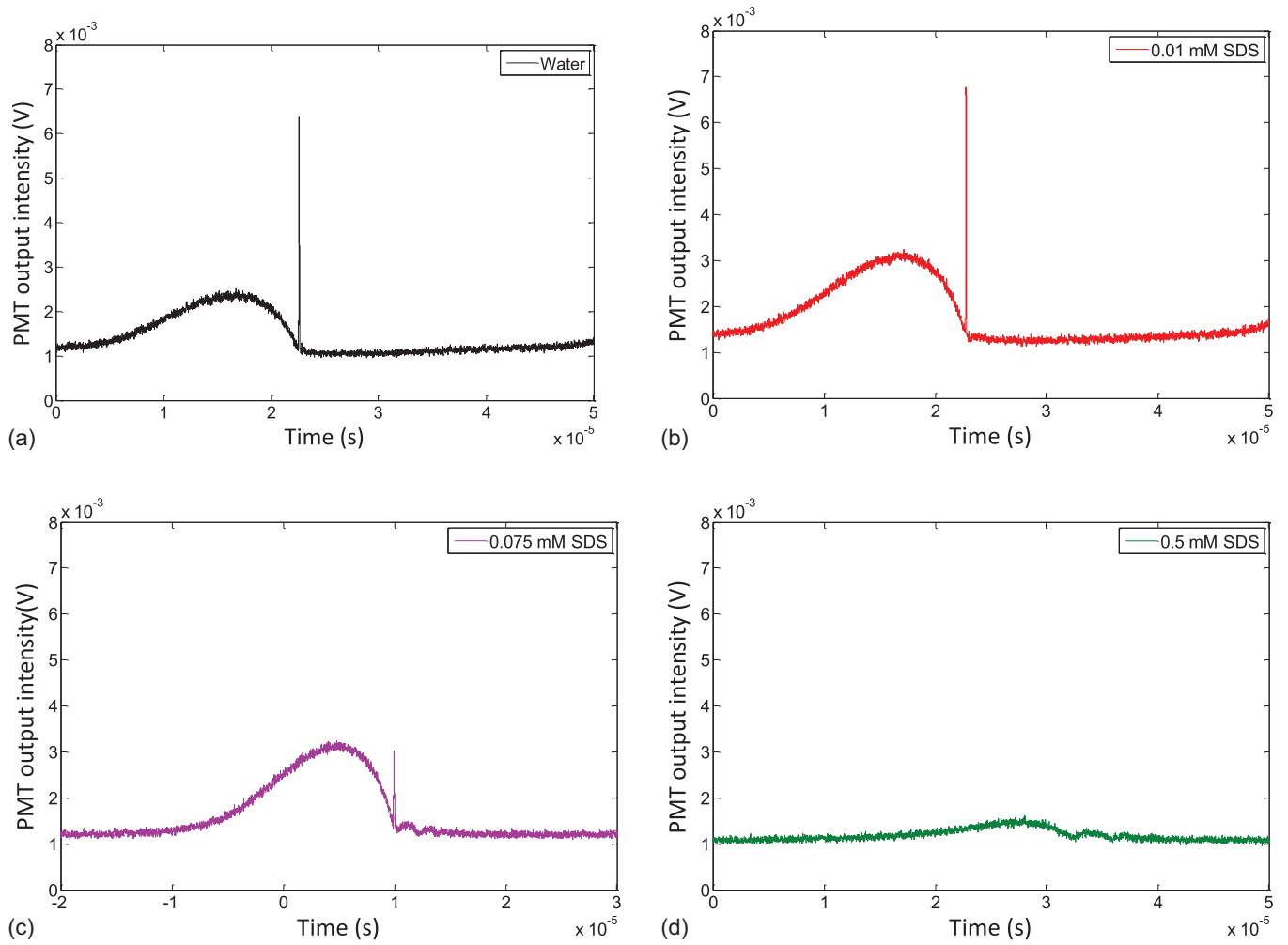


FIG. 5. (Color online) Plot of a typical PMT output curve for (a) water, (b) 0.01 mM SDS, (c) 0.075 mM SDS, and (d) 0.5 mM SDS obtained from experiments. At low concentrations, the SL and RT behavior is similar to water. As concentrations increase, the maximum radius of expansion and hence the SL yield becomes lower. Another noticeable trend with increasing concentration is that the size of the afterbounces relative to the main collapse increases.

of both stable and unstable behavior for an air bubble in water are shown in Fig. 3. Usually, stability can be determined from 20 to 30 periods (a period is the time for one full oscillation). In some cases, more than 100 periods are required to judge the stability. Calculations using conditions reported by Loughran *et al.* [51] for a shell-coated bubble are also consistent with these authors [Fig. 3(c)]. We validate the calculated numerical results for water with experimental results obtained from Holt and Gaitan [52], shown in Fig. 4. In this figure, the region below the solid line is the parameter space where a bubble is shape stable. The region above this is where the bubble is unstable for the $n = 2$ mode of oscillation, and agrees well with the data obtained by Holt and Gaitan. Similar agreement was obtained for Hao and Prosperetti [53] in their investigations.

VI. RESULTS AND DISCUSSION

A. Sonoluminescence in surfactant solutions

Typical PMT outputs obtained in a SBSL experiment are shown in Fig. 5. In these figures, the scattered laser intensity shows the radius-time (RT) behavior of the bubble as it undergoes violent collapse. The strong spike at the point of collapse that can be seen in Fig. 5 is due to the sonoluminescence (SL) emission.

At low surfactant concentrations the RT behavior and SL emission intensity are essentially the same as water. This has been shown previously by Ashokkumar *et al.* [54]. It can also be seen that there is actually a slight increase in the maximum radius and SL yield at very low SDS concentrations, consistent with the observations by Ashokkumar *et al.* Suzuki *et al.* also showed that bubbles became less prone to dancing motion in dilute solutions of SDS [55]. This trend is replicated in these current results at the lower surfactant concentrations investigated. As the concentration is increased, however, the RT behavior of the bubble begins to deviate from that shown in water. Lower maximum radii of expansion are observed, consistent with Stottlemyer and Apfel [19] and more distinct and somewhat broader afterbounces are observed after the main collapse. The results are also similar with those shown previously by Kozuka *et al.* [56] whereby the afterbounces become more pronounced relative to the main bubble collapse, with decreasing driving pressure. This suggests that the maximum pressure to which the bubble can be stably driven decreases with the addition of surfactant. A further increase in pressure causes the bubble to either disintegrate or to display dancing motion and move away from the antinode. This general trend can be seen more clearly in Fig. 6. The decrease of the maximum radius with increasing viscoelasticity can also be seen in the calculated radial dynamics shown in Fig. 7.

The consequence of the decrease in maximum radius is a decrease in the SL yield relative to water. Above a certain concentration of surfactant, the SBSL disappears entirely and can no longer be produced. This can be seen in the case of SDS, DTAC, and SDS with the addition of 0.1 mol/L NaCl in Fig. 8.

Figure 8 also shows that the addition of 0.1 mol/L NaCl to the solution causes a larger decrease in the SBSL than in the cases with no salt added at low bulk concentrations. The addition of 0.1 mol/L NaCl increases the surface activity of the

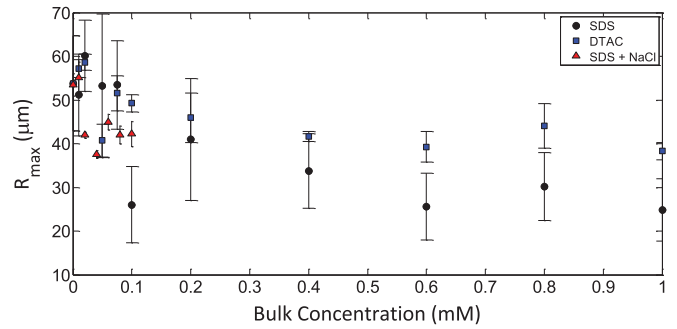


FIG. 6. (Color online) Plot of the maximum bubble radius obtained experimentally at high driving pressure (approximately 1.1–1.3 bars). As surfactant concentration is increased, the maximum radius that can be achieved is lowered. More surface active surfactants reduce the achievable R_{max} at lower bulk concentrations. Error bars are the standard deviation across a number of replicated experiments.

surfactant [21], and so for the same given bulk concentration, more surfactant will be present on the surface. A higher surface concentration results in a more viscoelastic surface. This along with the lower R_{max} of SDS with 0.1 mol/L NaCl shown in Fig. 6 supports the explanation that the decrease in the SBSL is due to higher surface viscoelastic effects that limit the oscillation amplitude of the bubble.

The compression ratio of the maximum radius to the minimum radius gives an indication of the intensity of the SBSL that can be achieved [37]. The ability of the bubble to undergo SBSL is related to the magnitude of the bubble collapse. This compression ratio is determined by the maximum bubble size (R_{max}) that the bubble can achieve during oscillation and the minimum bubble radius (R_{min}) during the collapse.

In Fig. 9, the SL intensity relative to water along with the trend in decrease of R_{max}/R_{min} is shown for SDS, DTAC, and SDS+salt. In all cases, the trend of decreasing SL intensity is accompanied with a decrease in the R_{max}/R_{min} ratios and an increase in the surfactant concentration.

The temperature of the bubble during collapse is also closely related to this R_{max}/R_{min} ratio. A lower maximum radius decreases the temperature achieved and also the number of excited electrons in the bubble core, which is predicted to

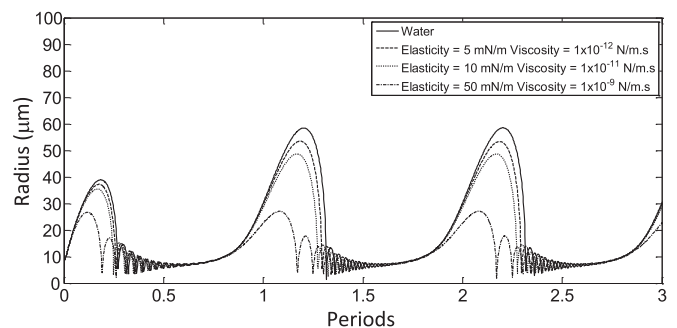


FIG. 7. Decrease in oscillation amplitude with increasing surface elasticity and viscosity determined from numerical calculations. Driving frequency of 20.6 kHz, $P_a = 1.3$ bars, and $R_0 = 10$ μm are used. Equilibrium surface tension of 73 mN/m used for water and 68 mN/m for the surfactants.

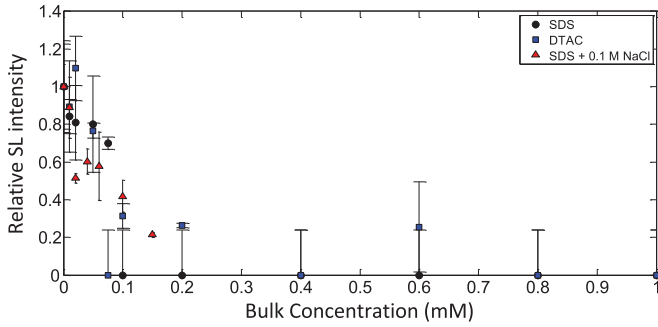


FIG. 8. (Color online) Decreasing SBSL intensity (relative to water) for SDS, DTAC, and SDS with 0.1 mol/L NaCl (approximately 1.1–1.3 bars) obtained experimentally. For SDS with the addition of 0.1 mol/L NaCl, a larger decrease in SBSL is seen due to a higher surface loading of surfactant at equivalent bulk concentration. DTAC is less surface active than SDS and so is able to sustain SL even at higher bulk concentrations. Error bars are the standard deviation across a number of replicated experiments.

decrease the intensity of emitted light [17]. Also as suggested by Yasui [20], the presence of surfactant on the surface of the bubble will also inhibit the condensation of water vapor during bubble collapse, further decreasing the bubble collapse temperature and hence SL intensity. The “trapping” of more water vapor and air molecules would cushion the collapse intensity and hence lower the maximum temperature and hence SL.

If this was occurring in our study at the surfactant concentration range used, one would expect the equilibrium radius to increase with an increase in the surfactant concentration. A higher internal pressure (due to trapped water vapor and air) would also mean an increase in R_{max} . However, the observations that (i) R_0 did not significantly change and (ii) there is a decrease in R_{max} with an increase in surfactant concentration, suggests that the contribution by vapor and gas to the observed effects may be insignificant under the experimental conditions used in this study.

The same is also true in multibubble systems, as reported by Lee *et al.* [57] No SL quenching was ever observed in the presence of surfactants. Instead, our previous investigations into the role of such soluble surfactants showed that they

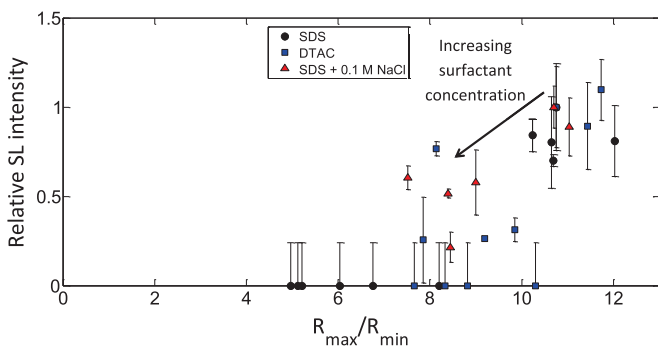


FIG. 9. (Color online) SBSL relative to water plotted as a function of the R_{max}/R_{min} ratio determined experimentally. SL intensity is reduced at lower R_{max}/R_{min} ratios, which occur at increasing surfactant concentrations. Error bars are the standard deviation across a number of replicated experiments.

primarily influenced the growth rate of bubbles by rectified diffusion [39,58]. We have shown previously that such surfactants inhibit the transfer of air across the air-liquid interface, leading to an enhancement in the rate at which the bubble grows in size [39]. Owing to the complexity of this problem, further study into the role of surfactants and their influence on both the rectified diffusion and trapping of water vapor is warranted, particularly at higher surfactant loadings.

Note also that the permeability of soluble surfactants, which form expanded interfaces such as those considered here due to diffusion, are relatively high. Values for the mass transfer resistance of air across such surfactant interfaces have been reported by Fyrrillas and Szeri [59]. These values are significantly different when compared with those of organic films such as long chain alcohols that form a “condensed” film on the surface of an air-water interface, as investigated by Davies *et al.* [60]. At high oscillation frequency, however, soluble surfactants approach behavior similar to condensed films since there is little time for relaxation to occur by

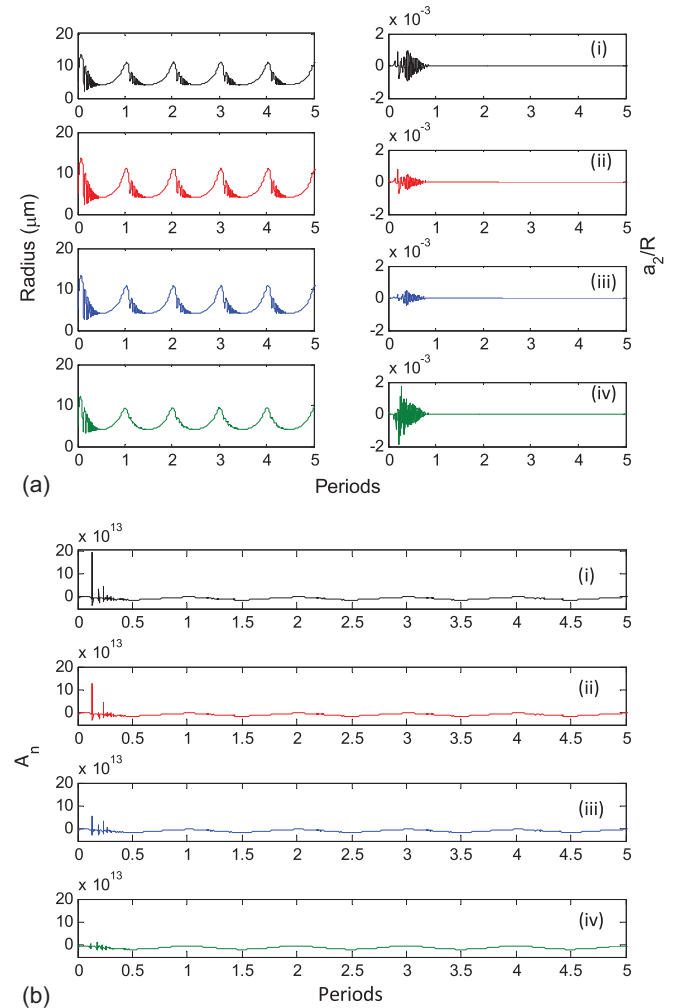


FIG. 10. (Color online) Effect of increasing surface elasticity: (i) 0 mN/m, (ii) 0.1 mN/m, (iii) 1.0 mN/m, and (iv) 10.0 mN/m at a surface dilatational viscosity of zero on the calculated (a) bubble radius and (b) A_n at a driving pressure of 1.0 bar and ambient radius of 5.0 μm .

diffusion. Water evaporation and adsorption are reportedly delayed by compressed, highly ordered films [43].

As above, the increase in surfactant concentration during SBSL experiments also leads to more observable dancing motion and bubble disintegration, evident of Rayleigh-Taylor instability. We continue this investigation in the following section to ascertain numerically the possible reasons for the observed decrease in stability.

B. The effect of surface viscoelasticity on radial oscillation and stability

In the driving pressure range and frequency investigated for SBSL, surface elasticity and/or viscosity (above a certain magnitude) causes a significant damping of the radial oscillations [Figs. 10(a) and 11(a)]. In general, this can also lead to an increase of the bubble stability. The elasticity can, however, lead to less damping if sufficiently high in magnitude, such as for the case of $\chi = 10$ mN/m.

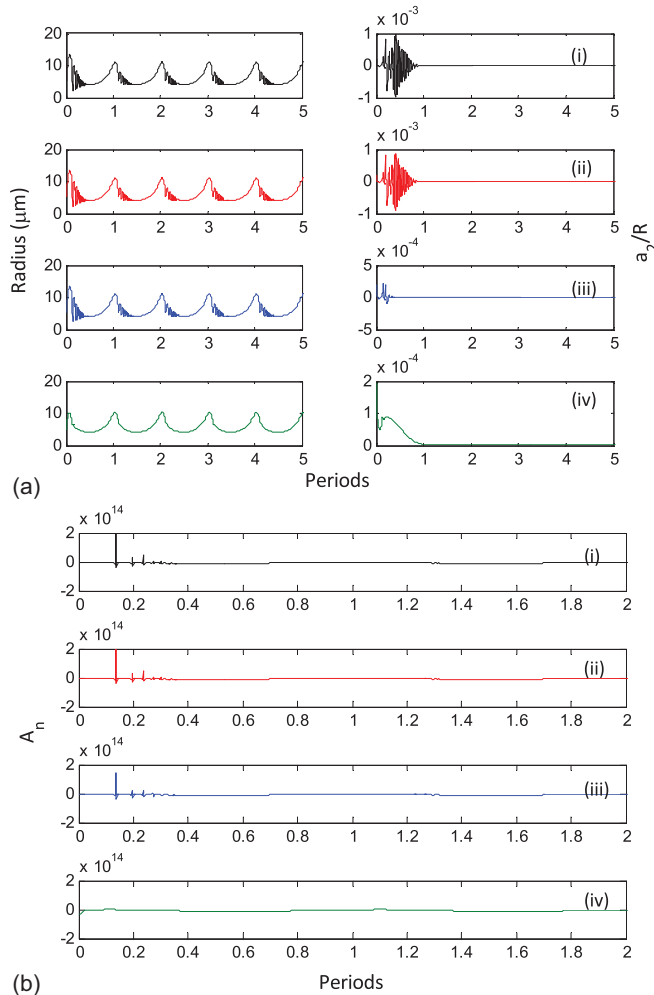


FIG. 11. (Color online) Effect of increasing surface dilatational viscosity for (i) 0 N/m s, (ii) 1×10^{-11} N/m s, (iii) 1×10^{-9} N/m s, and (iv) 1×10^{-7} N/m s at a surface elasticity of 0 mN/m on the calculated (a) bubble radius and dynamic stability at a driving pressure of 1.0 bar and ambient radius of $5.0 \mu\text{m}$. A_n is plotted as a function of the oscillation period in (b).

In the absence of viscoelasticity, i.e., in water, the calculated value of A_n [Eq. (25)] remains negative through most of the oscillation period owing to the effects of the equilibrium surface tension [second term of Eq. (25)] [Fig. 10(b)]. The exception is when the bubble undergoes strong collapse. At this point, A_n can become strongly positive as the acceleration [first term of Eq. (25)] and the velocity [third term of Eq. (25)] become large in magnitude and then suddenly change sign (i.e., acceleration followed by sudden deceleration). The result is a very sharp spike in the value of A_n in the positive direction. Parametric instability results from this spike in A_n as it results in an exponential increase of a_n . A higher elasticity reduces the magnitude of the positive spike in A_n [Fig. 10(b)] and its countering response ($A_n < 0$) is also lowered.

Increases in the surface dilatational viscosity dampen the instability of the initial perturbation with increasing strength as it reduces the amplitude of the radial-time oscillation.

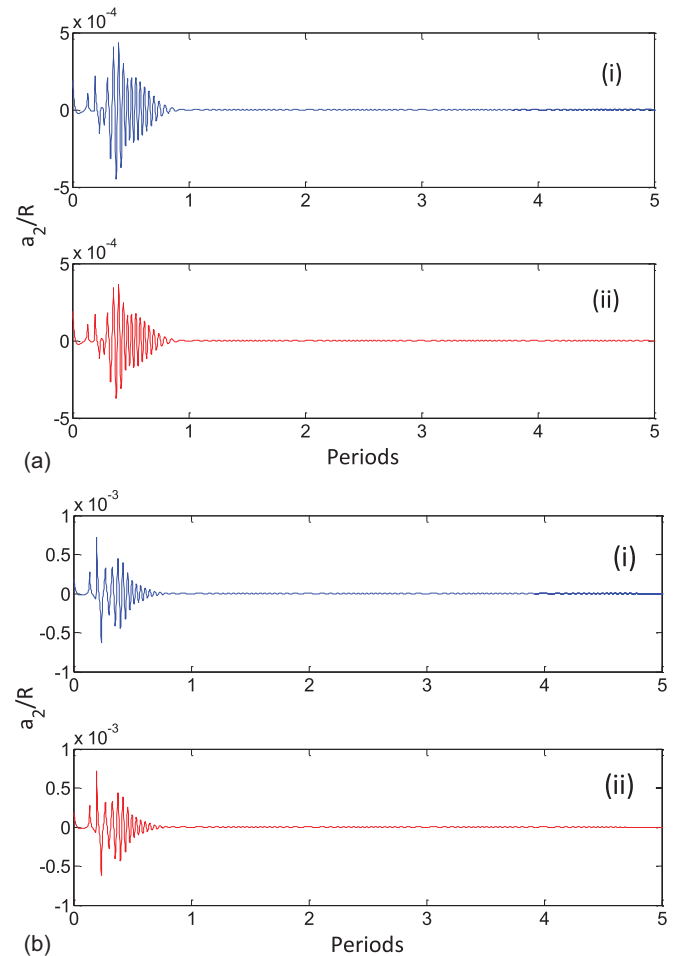


FIG. 12. (Color online) (a) The effect of including a surface shear modulus G_s on the calculated radial distortion amplitude at a surface elasticity of 1.0 mN/m and a surface dilatational viscosity of zero at a driving pressure of 1.0 bar and ambient radius of $5.0 \mu\text{m}$. (i) $G_s = 0$, (ii) $G_s = 0.25$ mN/m. (b) The effect of including a shear viscosity μ_s on the radial distortion amplitude at a surface dilatational viscosity of 1×10^{-10} N/m s and a surface elasticity of zero at a driving pressure of 1.0 bar and ambient radius of $5.0 \mu\text{m}$. (i) $\mu_s = 0$, (ii) $\mu_s = 0.25$ mN/m.

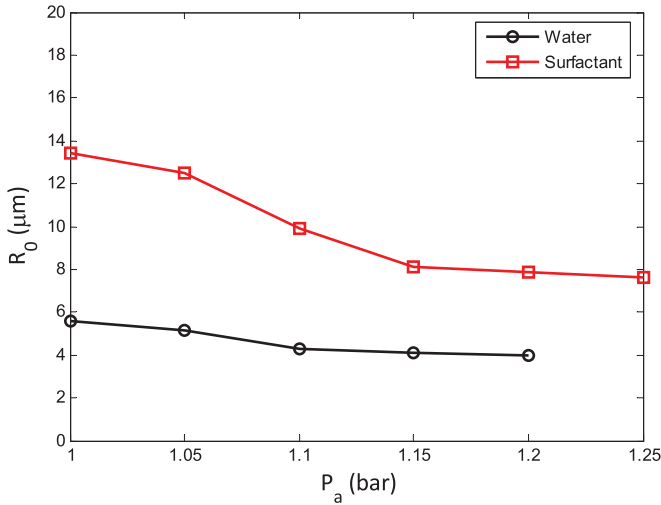


FIG. 13. (Color online) Calculated stability thresholds of the $n = 2$ mode for a surfactant-coated bubble with surface elasticity = 100 mN/m and surface dilatational viscosity of 1×10^{-10} N/m s compared with pure water. A surface tension of 50.0 mN/m is used for the surfactant-coated bubble and 73.0 mN/m is used for the clean bubble. In the case of the surfactant-coated bubble, G_s and μ_s are estimated to be 25% of the surface elasticity and viscosity, respectively. An acoustic driving frequency of 20.6 kHz is used.

Figure 11(b) shows that it not only decreases the magnitude to which A_n spikes during bubble collapse, but also increases its magnitude in the negative direction. The inclusion of either a surface shear modulus or shear viscosity, estimated as 25% of the surface elasticity and viscosity, respectively (Fig. 12), has minimal effect on the overall damping of the instability.

In Fig. 13, stability threshold curves are developed for a typical surfactant-coated bubble at a driving frequency of 20.6 kHz ($n = 2$ mode). In these plots, the effects of surface viscoelasticity on the stability of the bubble surface can be seen across a range of operating pressures. The curve produced is consistent with previous studies [55], in that the presence of surfactant makes a bubble more shape stable. However, even though the bubble is more “stable,” a decrease in the bubble’s ability to oscillate to the same maximum amplitude as a clean bubble makes it inherently more difficult to achieve SBSL.

Figure 14 shows the change in a_2/R and A_n with time for a clean and surfactant-coated bubble driven at 1.1 bars near their respective stability thresholds. This figure demonstrates that the surfactant-coated bubble is dominated by instability during the first bubble collapse only, giving rise to Rayleigh-Taylor instability. The Rayleigh-Taylor type of instability would be more likely to cause the bubble to undergo unstable dancing behavior as observed experimentally. In contrast, the clean bubble surface has instability resultant from the positive spiking which continues to propagate with time, leading to parametric instability.

An increase of the driving pressure to force the bubble to expand in amplitude often causes the bubble to become unstable, and this is observed experimentally by the strong dancing motion that has also been observed in this present

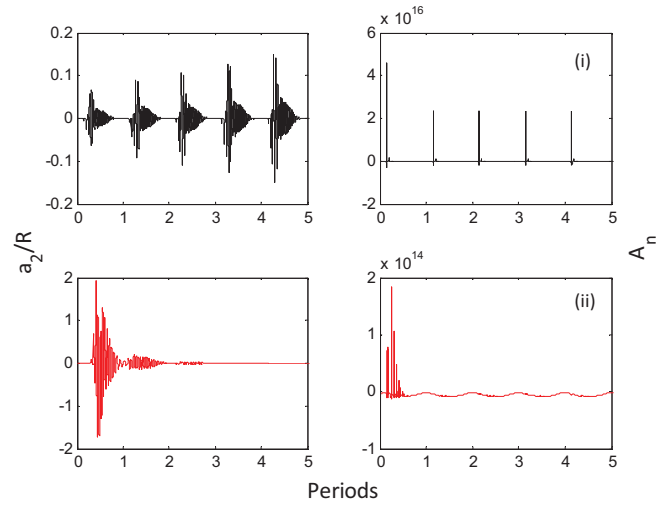


FIG. 14. (Color online) Radial distortion amplitude and A_n as a function of oscillation period calculated for (i) water and (ii) a surfactant-coated bubble (with the same properties as that in Fig. 13) driven at 1.1 bars, 20.6 kHz. The clean bubble is parametrically unstable while the surfactant-coated bubble is parametrically stable but Rayleigh-Taylor unstable.

study. In Fig. 15, the driving pressure amplitude is increased to 1.1 bars for a surfactant solution with lower surfactant concentrations than used in Fig. 13 (surface tension 68 mN/m, surface elasticity 10 mN/m, surface dilatational viscosity 1×10^{-11} N/m s). It is clear that the higher driving pressure required to achieve an equivalent radial amplitude to that observed in water causes the surfactant-coated bubble to become

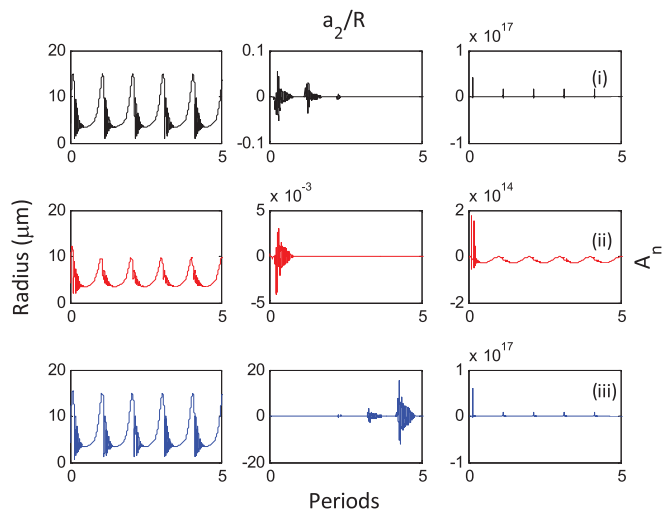


FIG. 15. (Color online) Radius, radial distortion amplitude, and A_n as a function of oscillation period of a bubble calculated in (i) water driven at 1.1 bars and surfactant solution driven at a pressure of (ii) 1.1 bars, and (iii) 1.208 bars. For the surfactant solution, the equilibrium surface tension = 68 mN/m, surface elasticity = 10 mN/m, and surface dilatational viscosity = 1×10^{-11} N/m s. An equilibrium surface tension of 73 mN/m is used for water. For all cases, the driving frequency is 20.6 kHz and an ambient radius of 4.25 μm is used.

shape unstable. However, in this case the instability is parametric, and so there is likely to be sufficient time (approximately ten cycles) for corrective mechanisms to bring the bubble into a regime where it can emit SBSL. One of the possible mechanisms for this correction is the readjustment of the ambient radius by enhanced diffusion during the nonspherical period of the bubble oscillation [61]. This demonstrates that SBSL emission is possible in the presence of less concentrated surfactant concentrations, as shown in the earlier experimental results.

VII. CONCLUSIONS

The radial oscillation of a sonoluminescing single bubble decreases in the presence of a surfactant. This decrease in oscillation also results in a decrease in emitted light intensity due to a lower temperature collapse. The viscoelastic properties of the surfactant layer contribute to these effects. A numerical study of the behavior of the bubble surface stability including the effect of surface viscoelasticity shows that in the 20 kHz frequency region, the presence of the surfactant reduces the oscillation amplitude and is the dominating effect that leads to a more stable bubble. However, this in turn reduces the SBSL intensity, and makes it practically more difficult to attain strong SBSL emission in concentrated surfactant solutions. An

increase in the driving pressure to induce SBSL in these cases can lead to Rayleigh-Taylor type instabilities, which in turn cause the bubble to enter into a chaotic state or to disintegrate completely.

It should be noted that our analysis assumes that neither shell buckling nor rupture occurs with such soluble surfactants. Further work is required to confirm whether this indeed is the case.

ACKNOWLEDGMENTS

The authors would like to acknowledge the Postgraduate Overseas Research Experience Scheme awarded by the University of Melbourne, the Research Travel Conference Assistance Scheme awarded by the School of Engineering (The University of Melbourne), the Travel Scholarship awarded by the Particulate Fluids Processing Centre (The University of Melbourne) and a Discovery grant from the Australian Research Council (DP0771094), which provided the funding that enabled this work to be performed. The National Institute of Advanced Industrial Science and Technology Chubu branch is also acknowledged for hosting the work.

-
- [1] D. F. Gaitan, L. A. Crum, C. C. Church, and R. A. Roy, *J. Acoust. Soc. Am.* **91**, 3166 (1992).
- [2] F. G. Blake, *J. Acoust. Soc. Am.* **21**, 551 (1949).
- [3] H. Lamb, *Hydrodynamics*, 5th ed. (Cambridge University Press, London, 1924).
- [4] F. R. Young, *J. Acoust. Soc. Am.* **60**, 100 (1976).
- [5] M. A. Beckett and I. Hua, *J. Phys. Chem. A* **105**, 3796 (2001).
- [6] R. Tronson, M. Ashokkumar, and F. Grieser, *J. Phys. Chem. B* **107**, 7307 (2003).
- [7] M. Ashokkumar, L. A. Crum, C. A. Frensley, F. Grieser, T. J. Matula, W. B. McNamara, and K. S. Suslick, *J. Phys. Chem. A* **104**, 8462 (2000).
- [8] K. Yasui, *J. Chem. Phys.* **116**, 2945 (2002).
- [9] G. J. Price, M. Ashokkumar, and F. Grieser, *J. Am. Chem. Soc.* **126**, 2755 (2004).
- [10] P. S. Epstein and M. S. Plesset, *J. Chem. Phys.* **18**, 1505 (1950).
- [11] N. Kamenka, B. Lindman, and B. Brun, *Colloid Polym. Sci.* **252**, 144 (1974).
- [12] S. Hilgenfeldt, D. Lohse, and M. P. Brenner, *Phys. Fluids* **8**, 2808 (1996).
- [13] W. Kloek, T. van Vliet, and M. Meinders, *J. Colloid Interface Sci.* **237**, 158 (2001).
- [14] R. B. Bird, W. E. Stewart, and E. N. Lightfoot, *Transport Phenomena*, 2nd ed. (John Wiley and Sons, New York, 2002).
- [15] C. C. Church, *J. Acoust. Soc. Am.* **84**, 1758 (1988).
- [16] B. D. Storey and A. J. Szeri, *Proc. R. Soc. London, Ser. A* **456**, 1685 (2000).
- [17] K. Yasui, T. Tuziuti, J. Lee, T. Kozuka, A. Towata, and Y. Iida, *J. Chem. Phys.* **128**, 184705 (2008).
- [18] K. Yasui, T. Tuziuti, M. Sivakumar, and Y. Iida, *J. Chem. Phys.* **122**, 224706 (2005).
- [19] T. R. Stottlemeyer and R. E. Apfel, *J. Acoust. Soc. Am.* **102**, 1418 (1997).
- [20] K. Yasui, *Phys. Rev. E* **58**, 4560 (1998).
- [21] M. J. Rosen, *Surfactants and Interfacial Phenomena*, 3rd ed. (John Wiley and Sons, New York, 2004).
- [22] Y. Jayalakshmi, L. Ozanne, and D. Langevin, *J. Colloid Interface Sci.* **170**, 358 (1995).
- [23] B. Dollet, S. M. van der Meer, V. Garbin, N. de Jong, D. Lohse, and M. Versluis, *Ultrasound Med. Biol.* **34**, 1465 (2008).
- [24] E.-A. Brujan, *Cavitation in Non-Newtonian Fluids: With Biomedical and Bioengineering Applications* (Springer, Berlin, 2010).
- [25] A. A. Doinikov and A. Bouakaz, *IEEE Trans. Ultrason., Ferroelectr., Freq. Control* **58**, 981 (2011).
- [26] A. Doinikov and P. Dayton, *Computational Methods in Multiphase Flow IV* (WIT Press, Southampton, Boston, 2007), p. 261.
- [27] K. Sarkar, W. T. Shi, D. Chatterjee, and F. Forsberg, *J. Acoust. Soc. Am.* **118**, 539 (2005).
- [28] D. Chatterjee and K. Sarkar, *Ultrasound Med. Biol.* **29**, 1749 (2003).
- [29] C. Church, *J. Acoust. Soc. Am.* **97**, 1510 (1995).
- [30] P. Marmottant, S. van der Meer, M. Emmer, M. Versluis, N. de Jong, S. Hildenfeldt, and D. Lohse, *J. Acoust. Soc. Am.* **118**, 3499 (2005).
- [31] K. Tsiglilis and N. A. Pelekasis, *J. Acoust. Soc. Am.* **123**, 4059 (2008).
- [32] Y. Liu, K. Sugiyama, S. Takagi, and Y. Matsumoto, *J. Fluid Mech.* **691**, 315 (2012).
- [33] Y. Liu, K. Sugiyama, S. Takagi, and Y. Matsumoto, *Phys. Fluids* **23**, 041904 (2011).
- [34] X. Lu, G. L. Chahine, and C.-T. Hsiao, *J. Acoust. Soc. Am.* **131**, 24 (2012).

- [35] T. G. Leighton, *The Acoustic Bubble* (Academic Press, San Diego, 1994).
- [36] M. Strasberg, *J. Acoust. Soc. Am.* **25**, 536 (1953).
- [37] M. P. Brenner, S. Hilgenfeldt, and D. Lohse, *Rev. Mod. Phys.* **74**, 425 (2002).
- [38] A. I. Eller and L. A. Crum, *J. Acoust. Soc. Am.* **47**, 762 (1970).
- [39] T. Leong, S. Wu, S. Kentish, and M. Ashokkumar, *J. Phys. Chem. C* **114**, 20141 (2010).
- [40] A. Bonfillon and D. Langevin, *Langmuir* **10**, 2965 (1994).
- [41] J. Lucassen and M. Van Den Tempel, *Chem. Eng. Sci.* **27**, 1283 (1972).
- [42] K.-D. Wantke, H. Fruhner, J. Fang, and K. Lunkenheimer, *J. Colloid Interface Sci.* **208**, 34 (1998).
- [43] S. Decesari, M. Facchini, M. Mircea, F. Cavalli, and S. Fuzzi, *J. Geophys. Res. Atmos.* **108**, 1984 (2003).
- [44] R. L. Kao, D. A. Edwards, D. T. Wasan, and E. Chen, *J. Colloid Interface Sci.* **148**, 247 (1992).
- [45] K. Yasui, *Phys. Rev. E* **56**, 6750 (1997).
- [46] L. Stricker, A. Prosperetti, and D. Lohse, *J. Acoust. Soc. Am.* **130**, 3243 (2011).
- [47] M. Spiegel, *Theory and Problems of Calculus of Finite Differences and Difference Equations (Schaum's Outline Series)* (McGraw-Hill Book Company, New York, 1971).
- [48] V. Kamath, A. Prosperetti, and F. N. Egolfopoulos, *J. Acoust. Soc. Am.* **94**, 248 (1993).
- [49] K. Yasui, *A New Formulation of Bubble Dynamics for Sonoluminescence* (Waseda University, Tokyo, 1996).
- [50] M. S. Plesset, *J. Appl. Phys.* **25**, 96 (1954).
- [51] J. Loughran, R. J. Eckersley, and M.-X. Tang, *J. Acoust. Soc. Am.* **131**, 4349 (2012).
- [52] R. G. Holt and D. F. Gaitan, *Phys. Rev. Lett.* **77**, 3791 (1996).
- [53] Y. Hao and A. Prosperetti, *Phys. Fluids* **11**, 1309 (1999).
- [54] M. Ashokkumar, J. Guan, R. Tronson, T. J. Matula, J. W. Nuske, and F. Grieser, *Phys. Rev. E* **65**, 046310 (2002).
- [55] H. Suzuki, I.-Y. S. Lee, and Y. Okuno, *Int. J. Phys. Sci.* **5**, 176 (2010).
- [56] T. Kozuka, S. Hatanaka, T. Tuziuti, K. Yasui, and H. Mitome, *Jpn. J. Appl. Phys.* **39**, 2967 (2000).
- [57] J. Lee, S. Kentish, T. J. Matula, and M. Ashokkumar, *J. Phys. Chem. B* **109**, 16860 (2005).
- [58] J. Lee, S. Kentish, and M. Ashokkumar, *J. Phys. Chem. B* **109**, 14595 (2005).
- [59] M. M. Fyrillas and A. J. Szeri, *J. Fluid Mech.* **289**, 295 (1995).
- [60] J. F. Davies, R. E. Miles, A. E. Haddrell, and J. P. Reid, *Proc. Natl. Acad. Sci. USA* **110**, 8807 (2013).
- [61] M. P. Brenner, D. Lohse, and T. F. Dupont, *Phys. Rev. Lett.* **75**, 954 (1995).